GEOPHYSICS, VOL. 67, NO. 4 (JULY-AUGUST 2002); P. 1115–1125, 12 FIGS.
10.1190/1.1500372

Localized *S*-inversion of time-domain electromagnetic data

Michael S. Zhdanov*, Dmitriy A. Pavlov*, and Robert G. Ellis‡

ABSTRACT

Interpretation of time-domain electromagnetic (TDEM) data over inhomogeneous geological structures is a challenging problem of geophysical exploration. The most widely used approach of interpreting TDEM data is based on the smooth 1-D layered resistivity inversion. We have developed an effective technique of fast TDEM inversion based on thin-sheet conductance approximation that we call *S*-inversion. In this paper we extend the *S*-inversion technique, approximating the conductivity cross-section by adding a local inhomogeneous disk with an excess conductance ΔS to the horizontal conductive thin sheet used in *S*-inversion. Localized *S*-inversion determines the distribution of this excess conductance as a function of a depth and a horizontal coordinate. This new method takes into account the limited horizontal extent of the inhomogeneities, localizing inversion. The numerical modeling results and inversion of practical TDEM data demonstrate that the method resolves local geological targets better than traditional 1-D inversion and original *S*-inversion. The method can be applied to interpret both ground and airborne TDEM data sets.

INTRODUCTION

Time-domain electromagnetic (TDEM) sounding is a powerful tool in mineral, geothermal, and groundwater exploration. It is widely used in ground and airborne observations. Several methods are available for interpreting TDEM data (Zhdanov and Keller, 1994). The traditional approach of approximating 1-D TDEM sounding interpretations uses the concept of apparent resistivity, based on a simple equivalent homogeneous half-space model. Apparent resistivity profiles provide a useful, quick analysis of TDEM data. Another common tool for TDEM data interpretation is based on 1-D layered model inversion. Several commercial software packages are available for TDEM interpretation that produce stitched cross-sections of smooth 1-D resistivity inversions.

Sidorov and Tikshaev (1969), Liu and Asten (1993), Tartaras and Zhdanov (1996), and Tartaras et al. (2000) have developed a method of inverting TDEM data, based on a thin-sheet approach. This method, which we call *S*-inversion, is based on an equivalent conductive thin sheet instead of the equivalent homogeneous half-space model used in the apparent resistivity definition. We can determine the apparent conductance $S_a(t)$ as the conductance of a thin sheet located at a depth d within a free space which generates a theoretical EM response equal to the observed TDEM response for some time moment t. This apparent conductance can be treated as the total conductance of the sequences of layers within the depth range of EM field penetration inside the earth for a given moment.

The smooth 1-D layered resistivity TDEM inversion and the original *S*-inversion method are limited because both methods do not account for the horizontal conductivity variations in geological structures. Localized *S*-inversion preserves the simplicity of *S*-inversion and, at the same time, provides a more adequate geoelectrical image of geological cross-sections by allowing for lateral variations in conductivity.

In this paper we modify the initial concept of the *S*-inversion. Our new approach is based on the following ideas.

In the first stage of interpretation, we apply the *S*-inversion thin-sheet approach to horizontally smoothed data and determine a cross-section of the apparent conductance (conductance as a function of the depth d of the corresponding thin sheet). We use this smoothed cross-section to establish the background conductance distribution $S_b(d)$, which corresponds to the points outside the conductivity anomalies.

In the second stage of interpretation, we introduce a new model of a thin conductive sheet with excess conductance $\Delta S =$ constant within a circular domain C_R with radius R and center located beneath the transmitter dipole. The total conductance S of this inhomogeneous thin sheet is represented by the sum

$$S = S_b + \Delta S.$$

Manuscript received by the Editor July 5, 2000; revised manuscript received November 16, 2001.
*University of Utah, Department of Geology and Geophysics, 135 South, 1460 East, #719, Salt Lake City, Utah 84112. E-mail: mzhdanov@mines.utah.edu; dapavlov@mines.utah.edu.
‡Minerals Exploration, BHP Billiton, 1111 W. Georgia St., Suite 1400, Vancouver, British Columbia V6E 4M3, Canada. E-mail: robert.g.ellis@bhpbilliton.com.

The radius R is determined according to the size of the corresponding current smoke rings generated by the transmitter at a depth d (Nabighian, 1979). The inversion now is reduced to determining the excess conductance ΔS from the observed TDEM data. Thus, in the framework of this approach, we represent the actual conductance cross-section as the superposition of the background conductance S_b and the anomalous conductance ΔS.

The main difference between this new approach and the original is that the background conductance may not equal zero. In other words, the host rocks can be conductive. Another advantage is that it is possible to find a quasi-analytical forward-modeling solution for this model which is fast enough for airborne data interpretation. Actually, in the framework of this approach, we can construct almost the same method as original S-inversion, with one very important difference. The new method would take into account a limited horizontal extent of the inhomogeneities, making the inversion local. That is why we call this method a localized S-inversion.

In the next sections we discuss the theory behind this approach and present some numerical results.

ELECTROMAGNETIC FIELD OVER A THIN CONDUCTING SHEET WITH A LOCAL CONDUCTIVE ANOMALY

We first examine the behavior of a step-induced transient magnetic field excited by a vertical magnetic dipole for a medium which consists of a single horizontal conductive sheet in an otherwise insulating full space. The thin sheet lies at depth d and has uniform integral conductance S_b (Figure 1). We assume that an EM field is caused by a current flowing in a loop of wire lying in the horizontal plane forming a vertical-axis magnetic dipole with a moment M at the surface of the earth. The waveform of the current flowing in the coil, I, is a Heaviside function $\mathcal{H}(t)$ (instantaneous change in level), or $I(t) = I_0\mathcal{H}(t)$. The Cartesian coordinate system originates below the transmitter at the depth of the thin sheet ($z = 0$), so the source coordinates are $(0, 0, -d)$. We also assume the magnetic permeability of the medium is equal to free space permeability μ_0.

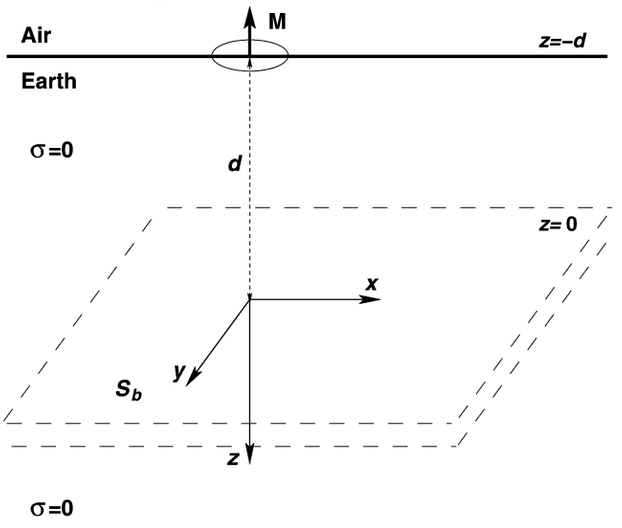

FIG. 1. Conductive thin sheet. The vertical magnetic dipole transmitter with a moment **M** is located at the surface of the earth.

The magnetic field at the surface of the earth ($z = -d$) caused by a source excited with a Heaviside (step on) waveform is (Zhdanov and Keller, 1994, p. 382)

$$H_z^{S_b}(t)\big|_{z=-d} = -\frac{M\mathcal{H}(t)}{4\pi}\frac{1}{r^3} + \frac{M}{4\pi}\frac{\left[r^2 - 8\left(d + \dfrac{t}{\mu_0 S_b}\right)^2\right]}{\left[r^2 + 4\left(d + \dfrac{t}{\mu_0 S_b}\right)^2\right]^{5/2}}, \quad (1)$$

where the first term represents the primary field, the second term describes the secondary field, and r is a horizontal distance from the source to the receiver.

We can also write an expression for the time derivative of the magnetic field because this physical quantity is usually measured with the induction coil receiver:

$$\frac{\partial H_z^{S_b}(t)}{\partial t}\bigg|_{z=-d} = \frac{M}{\pi\mu_0 S} \times \frac{\left(d + \dfrac{t}{\mu_0 S_b}\right)\left[-9r^2 + 24\left(d + \dfrac{t}{\mu_0 S_b}\right)^2\right]}{\left[r^2 + 4\left(d + \dfrac{t}{\mu_0 S_b}\right)^2\right]^{7/2}}, \quad t > 0. \quad (2)$$

Let us now assume that the thin conductive sheet has some excess conductance $\Delta S = \text{constant}$ within the circular domain C_R whose center is located just beneath the transmitter dipole in the origin of the coordinate (Figure 2). The total magnetic field in this case can be represented as the normal field, calculated above, and some anomalous field H_z^a:

$$H_z(x', y', t)|_{z=-d} = H_z^{S_b}(x', y', t)|_{z=-d} + H_z^a(x', y', t)|_{z=-d}, \quad (3)$$

where $(x', y', -d)$ are the coordinates of the observation point at the surface of the earth. The anomalous field can be described approximately as the field generated in free space by the excess currents

$$J_{x,y}^S(x, y, t) = \Delta S E_{x,y}(x, y, t), \quad (4)$$

flowing within the inhomogeneous domain C_R. In other words, we can use the Born approximation to calculate the anomalous magnetic field. The Born approximation has been widely used in inverse schemes because it provides a linearized approach to the solution of inverse problems (Oristaglio, 1989; Habashy et al., 1993). Our approach assumes there is negligibly small interaction between the excess currents within the local inhomogeneity and the homogeneous thin sheet. In this case we can use the Green's function for the free space. This means we can approximately estimate the anomalous field by the Biot–Savart law.

According to the Biot–Savart law, the vertical component of the anomalous field at the point $(x', y', -d)$ can be computed as

$$H_z^a(t)\big|_{z=-d} = \frac{1}{4\pi} \times \iint_{C_R} \frac{(x-x')J_y^S(x,y,t) - (y-y')J_x^S(x,y,t)}{\left[(x-x')^2 + (y-y')^2 + d^2\right]^{3/2}}\, dx\, dy. \tag{5}$$

In the Appendix we demonstrate that the electric-field components over a thin conductive sheet are defined by symmetrical equations:

$$E_x(x,y,t) = \frac{3M}{2\pi S_b} d_\tau \left(x^2 + y^2 + d_\tau^2\right)^{-5/2} y,$$
$$E_y(x,y,t) = -\frac{3M}{2\pi S_b} d_\tau \left(x^2 + y^2 + d_\tau^2\right)^{-5/2} x, \tag{6}$$

where

$$d_\tau = d + \frac{2t}{\mu_0 S_b}. \tag{7}$$

Substituting equations (4) and (6) into equation (5), we find

$$H_z^a(t)\big|_{z=-d} = \frac{3\Delta SM}{8\pi^2 S_b} d_\tau \times \iint_{C_R} \frac{-(x-x')x - (y-y')y}{\left[(x-x')^2 + (y-y')^2 + d^2\right]^{3/2}} \times \left(x^2 + y^2 + d_\tau^2\right)^{-5/2} dx\, dy. \tag{8}$$

We can also find the time derivative of the vertical magnetic-field component by differentiating formula (8):

$$\frac{\partial H_z^a(t)}{\partial t}\bigg|_{z=-d_0} = \frac{3\Delta SM}{4\pi^2 S_b^2} \times \iint_{C_R} \frac{-(x-x')x - (y-y')y}{\left[(x-x')^2 + (y-y')^2 + d^2\right]^{3/2}} \left[\left(x^2 + y^2 + d_\tau^2\right)^{-5/2}\right] \times \left[1 - \frac{5d_\tau^2}{(x-x')^2 + (y-y')^2 + d_\tau^2}\right] dx\, dy. \tag{9}$$

Using the same approach, we can find formulas for an airborne EM array with different elevations for the transmitter and receiver. If the transmitter level is $z = -d - d_s$ and the receiver level is $z = -d - d_r$ (Figure 3), the magnetic field can be computed using the following expressions:

$$H_z^a(t)\big|_{z=-d-d_r} = \frac{3\Delta SM}{8\pi^2 S_b} \tilde{d}_\tau \times \iint_{C_R} \frac{-(x-x')x - (y-y')y}{\left[(x-x')^2 + (y-y')^2 + (d+d_r)^2\right]^{3/2}} \times \left(x^2 + y^2 + \tilde{d}_\tau^2\right)^{-5/2} dx\, dy \tag{10}$$

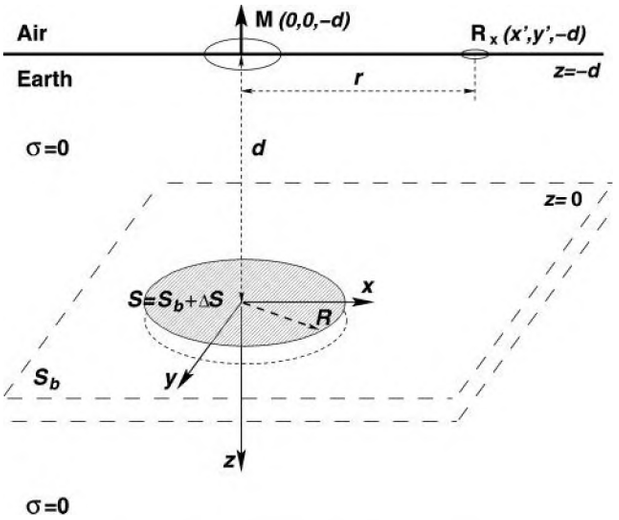

FIG. 2. A horizontal conductive thin sheet consisting of a homogeneous background part with conductance S_b and an inclusion formed by a local conductive disc with excess conductance ΔS. The vertical magnetic dipole transmitter with a moment **M** is located at the surface of the earth at a point $(0, 0, -d)$. The receiver $\mathbf{R}_x$ is located at the observation point $(x', y', -d)$ at the surface of the earth. The transmitter–receiver separation is r.

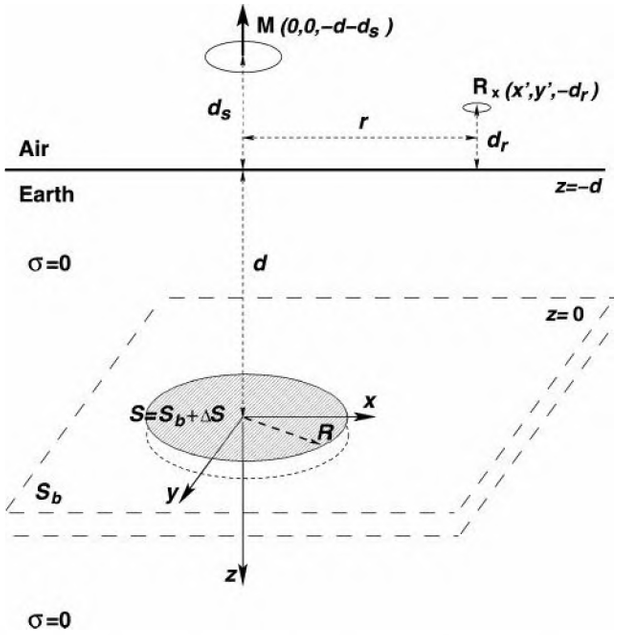

FIG. 3. A horizontal conductive thin sheet consisting of a homogeneous background part with conductance S_b and an inclusion formed by a local conductive disc with excess conductance ΔS. The transmitter and receiver are at different elevations. The vertical magnetic dipole transmitter is located at the level d_s above the earth's surface. The receiver is located at the level d_r above the earth's surface. The transmitter–receiver separation is r.

and

$$\left.\frac{\partial H_z^a(t)}{\partial t}\right|_{z=-d-d_r} = \frac{3\Delta S M}{4\pi^2 S_b^2} \times \iint_{C_R} \frac{-(x-x')x-(y-y')y}{\left[(x-x')^2+(y-y')^2+(d+d_r)^2\right]^{3/2}} \times \left[\left(x^2+y^2+\tilde{d}_\tau^2\right)^{-5/2}\right] \times \left[1-\frac{5\tilde{d}_\tau^2}{(x-x')^2+(y-y')^2+\tilde{d}_\tau^2}\right] dx\,dy, \tag{11}$$

where

$$\tilde{d}_\tau = d + d_s + \frac{2t}{\mu_0 S_b}$$

and where d_s and d_r are the elevations of the source and receiver above the earth's surface, correspondingly (Figure 3).

It is well known that the Born approximation works reasonably well only for relatively small conductivity contrasts and relatively small inhomogeneities. In our case we have a specific model of a thin, conductive disk located within a thin, conductive sheet. The maximum distance between any two points belonging to the disk is equal to its diameter. In this situation one could expect that the accuracy of the Born approximation would deteriorate with increasing diameter of the conductive disk.

We run a simple test to analyze the Born approximation errors. First, we compute the time derivative of the magnetic field, $\partial H_z^a(t)/\partial t$, using approximate formula (8) for the anomalous field generated by a horizontal conductive disk with the anomalous conductance ΔS and the radius $R_1 = 10d$. Second, we calculate the difference between the responses of two horizontal sheets with the uniform conductances of $S_b + \Delta S$ and S_b,

$$\frac{\partial H_z^d(t)}{\partial t} = \frac{\partial H_z^{S_b+\Delta S}(t)}{\partial t} - \frac{\partial H_z^{S_b}(t)}{\partial t},$$

using exact analytical solutions for a homogeneous thin sheet (2). The difference between these two solutions for every time moment is normalized by theoretical response $\partial H_z^{S_b}(t)/\partial t$ from the horizontal sheet with uniform integral conductance S:

$$\varepsilon(t) = \frac{\left|\frac{\partial H_z^a(t)}{\partial t} - \frac{\partial H_z^d(t)}{\partial t}\right|}{\left|\frac{\partial H_z^{S_b}(t)}{\partial t}\right|}. \tag{12}$$

Function $\varepsilon(t)$ can be treated as an approximate upper bound of the relative Born approximation errors for thin, conductive disks with the radii $<10d$ because we know the accuracy of this approximation increases for the disks with the smaller diameters. Figure 4 presents the plots of ε versus observation time for different ratios $\Delta S/S_b$. Typically, $\varepsilon(t) \le 0.1\Delta S/S_b$, and its maximum value at the late time does not exceed the ratio $\Delta S/S_b$. Thus, we conclude that the maximum relative errors of the Born approximation for the model of thin, conductive disk with the anomalous conductance ΔS within the homogeneous horizontal conductive S-sheet are less than $\Delta S/S_b$. In practical implementation of the localized S-inversion, we usually consider relatively small excess conductance in comparison with the background conductance. Thus, we can conclude that the approach based on the Born approximation is a reasonable model for fast inverse imaging of TDEM data.

PRINCIPLES OF LOCALIZED S-INVERSION

The localized S-inversion method consists of two interpretation steps.

In the first step we determine the observed anomalous magnetic-field derivative $\partial H_z^{a0}(t)/\partial t$ and the background conductance distribution $S_b(d)$ of the geoelectrical cross-section. To solve this problem, we calculate the background magnetic-field derivative $\partial H_z^b(t)/\partial t$ by filtering $\partial H_z^0(t)/\partial t$ to smooth lateral variations at all points of measurement along a profile for each time moment of the observations. We also note that the basic interpretation model of the localized S-inversion is formed by a local conductive disk. Within the framework of this model, the anomalous magnetic field derivative $\partial H_z^{a0}(t)/\partial t$ must be a local function itself, i.e., it must go to zero at the ends of the observation profile. That is why the lateral filtering also subtracts the linear trend from the observed data.

This procedure consists of four steps. First, the observed field derivative $\partial H_z^0(t)/\partial t$ is differentiated twice with respect to x:

$$f(x) = \frac{\partial^2}{\partial x^2}\left[\frac{\partial H_z^0(t)}{\partial t}\right].$$

The horizontal differentiation eliminates any linear trend in the observed data. Second, the function $f(x)$ is convolved with a Hanning filter, $h(x) = 0.5 - 0.5\cos(2\pi x/X)$, where X is the width of the filter, to give

$$p(x) = f(x) * h(x).$$

The convolution results in the smoothing of the second horizontal derivative. The width of the Hanning filter determines both the extent and amount of lateral smoothing along the profile, which makes the Hanning filter application convenient for our problem. Third, the second horizontal derivative $g(x)$ of the observed anomalous field is computed as the difference between $f(x)$ and its convolution with the Hanning filter:

$$g(x) = f(x) - p(x).$$

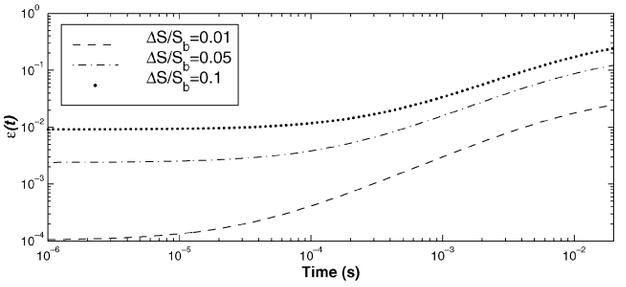

FIG. 4. Plots of an approximate upper bound of the relative Born approximation errors ε versus observation time for different ratios $\Delta S/S_b$.

Finally, we double integrate the field $g(x)$ to reconstruct an observed anomalous field $\partial H_z^{a0}(t)/\partial t$ from its second derivative:

$$\frac{\partial H_z^{a0}(t)}{\partial t} = \int \left(\int g(x)\,dx \right) dx + c_1 x + c_0.$$

The integration constants c_1 and c_0 are selected from the condition that the anomalous field is required to equal zero at the ends of the profile.

All of these procedures separate the observed magnetic-field derivative $\partial H_z^0(t)/\partial t$ into a background field $\partial H_z^b(t)/\partial t$ and an anomalous part $\partial H_z^{a0}(t)/\partial t$:

$$\frac{\partial H_z^0(t)}{\partial t} = \frac{\partial H_z^b(t)}{\partial t} + \frac{\partial H_z^{a0}(t)}{\partial t}. \tag{13}$$

The background field is slowly changing along the x-axis part of the observed magnetic-field derivative. The background field determined for all observed time moments is used to find the background conductance distribution $S_b(d)$ by the original S-inversion technique (Tartaras et al., 2000).

The background conductance distribution can also be obtained by smoothing the conductance $S(d)$ generated by S-inversion of the total observed data. However, we still need to find the background magnetic-field derivative to calculate the observed anomalous field, according to formula (13). This requires additional forward modeling calculations, which could be extremely time consuming. That is why we directly apply smoothing to the observed data in our localized S-inversion scheme to generate the background magnetic-field derivatives.

In the second stage of interpretation, we introduce the localized S-inversion model, which includes a thin, conductive sheet with excess conductance $\Delta S =$ constant within the circular domain C_R whose center is located beneath the transmitter dipole. Therefore, the total conductance S of this inhomogeneous thin sheet is represented by a sum $S = S_b + \Delta S$. For the selected time window of the TDEM sounding, we assume that the depth of the equivalent inhomogeneous thin sheet is equal to the depth of the thin sheet determined in the homogeneous S-inversion. The conductance of the homogeneous part of the inhomogeneous thin sheet is taken equal to the corresponding background conductance at this depth $S_b(d)$.

The radius R of the local inhomogeneity is determined according to the size of the corresponding smoke ring at d. Nabighian (1979) demonstrates that the transient response from the magnetic dipole over a conductive half-space can be represented approximately by a system of circular linear currents, resembling a system of smoke rings blown by the transmitter loop, which move downward with the velocity $V = 2/\sqrt{\pi\sigma\mu_0 t}$. The radius of the rings increases with time as $R = 4\sqrt{(4-\pi)t/\pi\sigma\mu_0}$. Using these formulas, one can obtain the connection between the radius of the ring and its depth:

$$R = z\sqrt{4-\pi}, \tag{14}$$

where $z = \int V dt = 4\sqrt{t/\pi\sigma\mu_0}$.

This result shows that function $R(z)$ does not depend on conductivity of the media. We use formula (14) to determine the radius of the local anomalous domain within the conductive thin sheet.

The localized S-inversion is reduced to determining the excess conductance ΔS from the observed TDEM data. For the selected time window on the TDEM sounding curve, we determine the observed anomalous field $\partial H_z^{a0}(t)/\partial t$, using the technique described above. To find the excess conductance generating the theoretical anomalous field, $\partial H_z^a(t)/\partial t$, which better approximates the observed anomalous field, $\partial H_z^{a0}(t)/\partial t$, we fit the anomalous data observed at adjacent time channels, using the theoretical data computed by equation (9). Since we invert for one parameter, ΔS, we can use data just from one time channel for each inversion. However, to make the solution more stable in the presence of noise, we select several adjacent time channels (usually four or five) that form a sliding time window $(t - \Delta t/2, t + \Delta t/2)$, where Δt is the width of the window (Figure 5). Every fixed position of the sliding window center t corresponds to the specific depth z of the EM-field penetration in the earth and to the specific depth d of the conductive thin sheet determined by S-inversion (Tartaras et al., 2000). When we move the sliding time window to later times, the depth of the corresponding thin sheet d monotonically increases. For every position of the sliding time window, we numerically solve the inverse problem for the anomalous field $\partial H_z^{a0}(t)/\partial t$ and find the excess conductance of the corresponding thin sheet, $\Delta S(d)$.

We use the adaptive regularized conjugate-gradient method to solve the inverse problem (Zhdanov and Keller, 1994). It is based on minimizing the parametric functional, P^α:

$$P^\alpha(\Delta S) = \phi(\Delta S) + \alpha s(\Delta S) = \min, \tag{15}$$

which is a linear combination of the misfit functional $\phi(\Delta S)$,

$$\phi(\Delta S) = \left\| \frac{\partial H_z^{a0}(t)}{\partial t} - \frac{\partial H_z^a(t)}{\partial t} \right\|^2, \tag{16}$$

and a stabilizing functional $s(\Delta S)$

$$s(\Delta S) = \|\Delta S - \Delta S_{apr}\|^2. \tag{17}$$

In Equations (15) and (16) α is the regularization parameter, ΔS_{apr} is the a priori model, and $\|\ldots\|$ denotes the least-squares norm. Functional (17) is selected to be equal to the conventional minimum norm stabilizer if there is no prior information available (Zhdanov and Keller, 1994):

$$s(\Delta S) = \|\Delta S\|^2.$$

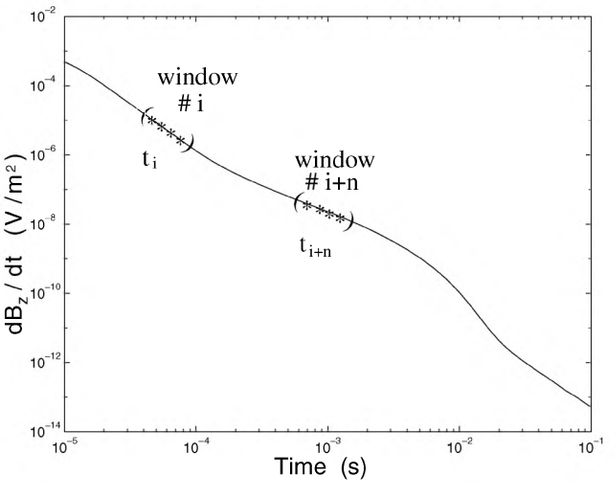

FIG. 5. Sliding time windows.

We use the conjugate gradient method to minimize the parametric functional (Zhdanov, 1993). The iteration process is automatically terminated when the normalized misfit reaches the desired value.

The Frechet derivative matrix, required for conjugate gradient algorithm, is composed of partial derivatives of the data with respect to the model parameters. Thus, the Frechet matrix is an $N_d \times N_m$ matrix, where N_d is the number of data points used and N_m is the number of model parameters. Therefore, in our case the Frechet matrix is a 5×1 matrix, since we have only one parameter, anomalous conductance ΔS, and usually use five data points.

An important problem is calculating the appropriate value of the regularization parameter α. We use an adaptive regularization, which is based on scaling down α after several subsequent iterations (Zhdanov, 1993). If the misfit value increases, the value of α decreases and the iteration step is repeated.

Another critical question in implementing the regularized inversion method is selecting the starting model. In the case of localized S-inversion, a natural choice for the starting value of ΔS is zero.

As a result of the localized S-inversion, we plot the cross-section of the anomalous conductance ΔS versus depth d. Some numerical results are presented in the next section.

NUMERICAL RESULTS

We developed a computer program to implement localized S-inversion and tested it on numerous synthetic data sets. The synthetic data (dB_z/dt values) were generated by the 3-D EM modeling code SYSEM, which is based on the integral equations method (Xiong, 1992). The transmitter was approximated by a vertical magnetic dipole located 100 m above the earth's surface. The receiver was a vertical magnetic dipole located 130 m from the transmitter center and 50 m above the ground (Figure 6). The computed synthetic data were contaminated by 10% random noise.

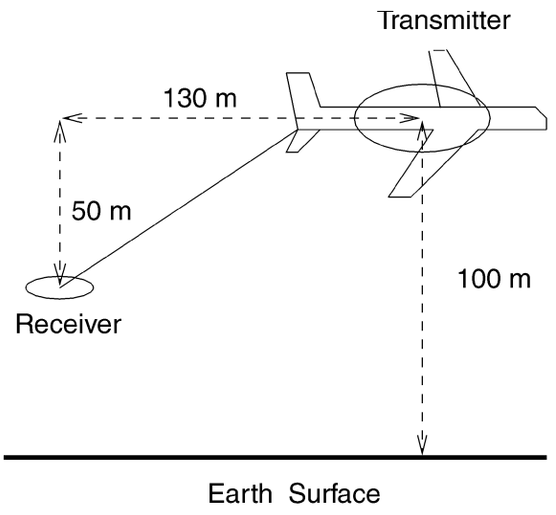

FIG. 6. Configuration of the airborne EM survey.

The localized S-inversion was applied to the data set at every receiver location. The resulting apparent conductance and apparent conductivity values were linearly interpolated and then plotted as conductance and conductivity pseudosections.

Figure 7 shows one geoelectrical 3-D model used in this study. It consists of a thick $200 \times 400 \times 100$-m body with a resistivity of 1 ohm-m located 100 m below the surface in a homogeneous half-space with a resistivity of 100 ohm-m. The observations were simulated for the slingram mode, with the receiver and transmitter moving along the profile passing above the center of the 3-D structure. The measurements were taken every 25 m. Figure 8a shows the result of the conventional smooth 1-D conductivity inversion, generated by Airstem code (Ellis, 1998a,b). The horizontal extent of the conductive body is exaggerated in this image. The apparent conductance and apparent conductivity cross-sections obtained by traditional S-inversion are presented in Figures 8b,c. As shown in Figure 8b, the position of the top of the body is well resolved, but the rest of the underlying body is not resolved, as usually happens with conductance images. The conductivity image in the third panel from the top is distorted by the noise. One can see only an unfocused mosaic pattern in the place of the actual body. Figure 8d shows the anomalous conductance distribution obtained as a result of the localized S-inversion. The thick conductive body is clearly observed. The image shows the correct position of the central part of the conductive body and the correct horizontal extension of the body. This result illustrates the stability of the localized S-inversion with respect to the noise in the data. Unfortunately, the conventional S-inversion lacks this stability.

Model 2 is shown in Figure 9. It consists of two $200 \times 400 \times 100$-m conductive bodies with a resistivity of 1 ohm-m embedded in a homogeneous earth with a resistivity of 100 ohm-m. The first body lies at a depth of 130 m and the second lies at a depth of 100 m from the surface. The distance between them is 300 m. The observations were simulated for the slingram mode, with the receiver and transmitter moving along the profile passing above the center of the 3-D structure. The measurements were taken every 25 m. Figure 10a presents the results of the conventional smooth 1-D inversion. Once again, the horizontal extent of the conductive body is slightly exaggerated. Actually, we can see a conductive belt in place of two conductive bodies. Figures 10b,c present the results of conventional S-inversion (conductance depth and conductivity depth cross-sections) obtained from the noisy data. The two conductive bodies are not resolved in these images because of the very

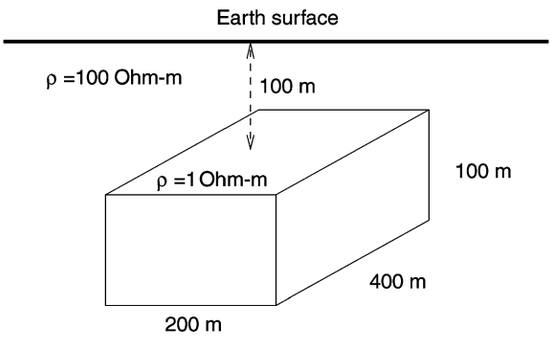

FIG. 7. Three-dimensional geoelectrical model 1.

high noise in the simulated data. This result can be explained; calculating the conductivity cross-section by differentiating the conductance cross-section is a very unstable procedure and is sensitive to data noise. The localized *S*-inversion for anomalous conductance is much more stable with respect to the noise in the data, as shown in Figure 10. Figure 10d shows that the anomalous conductance outlines the locations of both targets well.

In summary, the localized *S*-inversion is much more stable with respect to data noise than the conventional thin-sheet approach to inverting for conductivity. At the same time, the localized *S*-inversion resolves the local geoelectrical targets better than original *S*-inversion. The traditional 1-D inversion does a good job; however, it produces horizontally extended images.

EFFECT OF THE SIGNAL WAVEFORM ON THE LOCALIZED *S*-INVERSION

The synthetic data for numerical testing considered in the previous section were simulated by using a simple step waveform for the source. However, the localized *S*-inversion can be applied for processing data collected using any transmitter signal waveform. The current technology of airborne observations includes recording the signal waveform $w(t)$ by measuring the normalized primary magnetic-field component at the high elevation of the plane when the surrounding medium can be treated as a free space with

$$w(t) = \frac{\partial \tilde{H}_z^p(t)}{\partial t}. \tag{18}$$

The corresponding observed field can be represented, in this case, as the convolution between this primary field and some

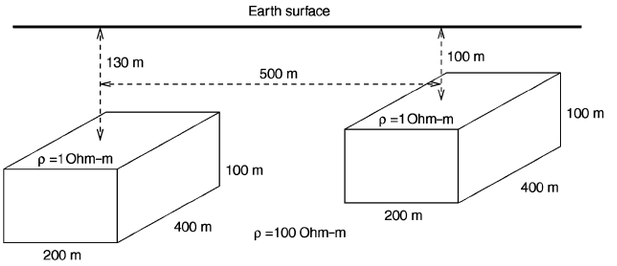

FIG. 9. Three-dimensional geoelectrical model 2.

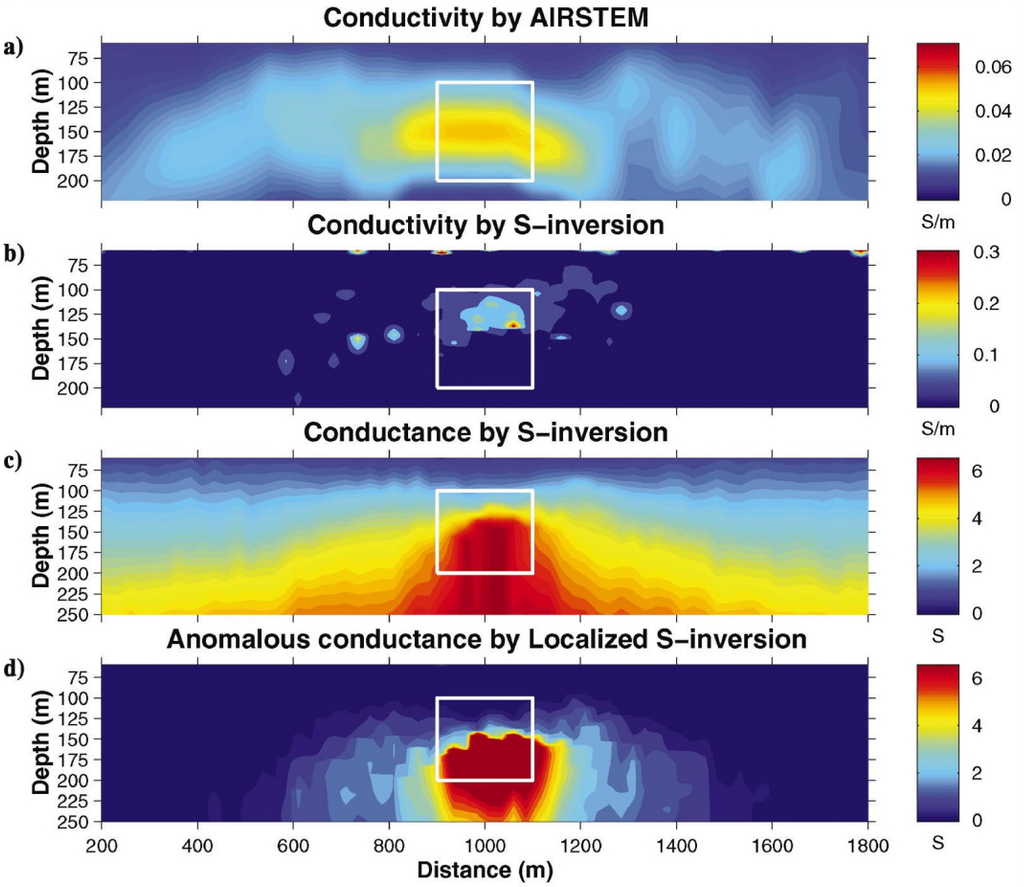

FIG. 8. Results of 1-D inversion, *S*-inversion, and localized *S*-inversion for model 1. (a) Result of the conventional smooth 1-D inversion by Airstem code. (b) Conductance cross-section by *S*-inversion. (c) Conductivity cross-section by *S*-inversion. (d) Anomalous conductance cross-section by localized *S*-inversion.

time characteristic $g(t)$ of the medium:

$$\frac{\partial H_z^{obs}(t')}{\partial t} = \int_0^T g(t-t')\frac{\partial \tilde{H}_z^p(t)}{\partial t}\,dt = \int_0^T g(t-t')w(t)\,dt. \quad (19)$$

In the case of a step current in the transmitter, the normalized primary field behaves as a delta function:

$$\frac{\partial \tilde{H}_z^p(t)}{\partial t} = \delta(t). \quad (20)$$

So the theoretical observed field for the step signal in the transmitter can be treated as the time characteristic of the thin-sheet model:

$$\frac{\partial H_z^H(t')}{\partial t} = \int_0^T g(t-t')\,\delta(t)\,dt = g(t-t'). \quad (21)$$

The simplest and most efficient approach to localized S-inversion is based on generating the theoretical fields for an infinitely long horizontal thin sheet and the local conductance anomaly as the convolution between the theoretical solutions obtained above [formulas (1), (9), and (11)] and the waveform corresponding to the data acquisition system:

$$\left.\frac{\partial H_z^{wtheor}(t)}{\partial t}\right|_{z=-d_0} = \int_0^T \frac{\partial H_z^H(t-t')}{\partial t}w(t)\,dt. \quad (22)$$

The numerical data simulated for a given waveform are used in inversion for conductance and depth of the equivalent thin sheet and for determining the excess conductance of the local anomaly within the sheet. In this way we avoid a complicated process of converting the observed field into a response for some specific transmitter waveform, which could increase the noise level in the data.

REAL DATA APPLICATION

We have applied the new localized S-inversion technique to a real data set provided by BHP Minerals. The TDEM data were collected using the Geotem system in the Bull Creek prospect located in North-West Queensland, Australia (Hart and Lane, 2001). The main exploration target in the Bull Creek prospect is the magnetite–pyrrhotite mineralization zone of Proterozoic age buried beneath a 30–50-m-thick conductive overburden.

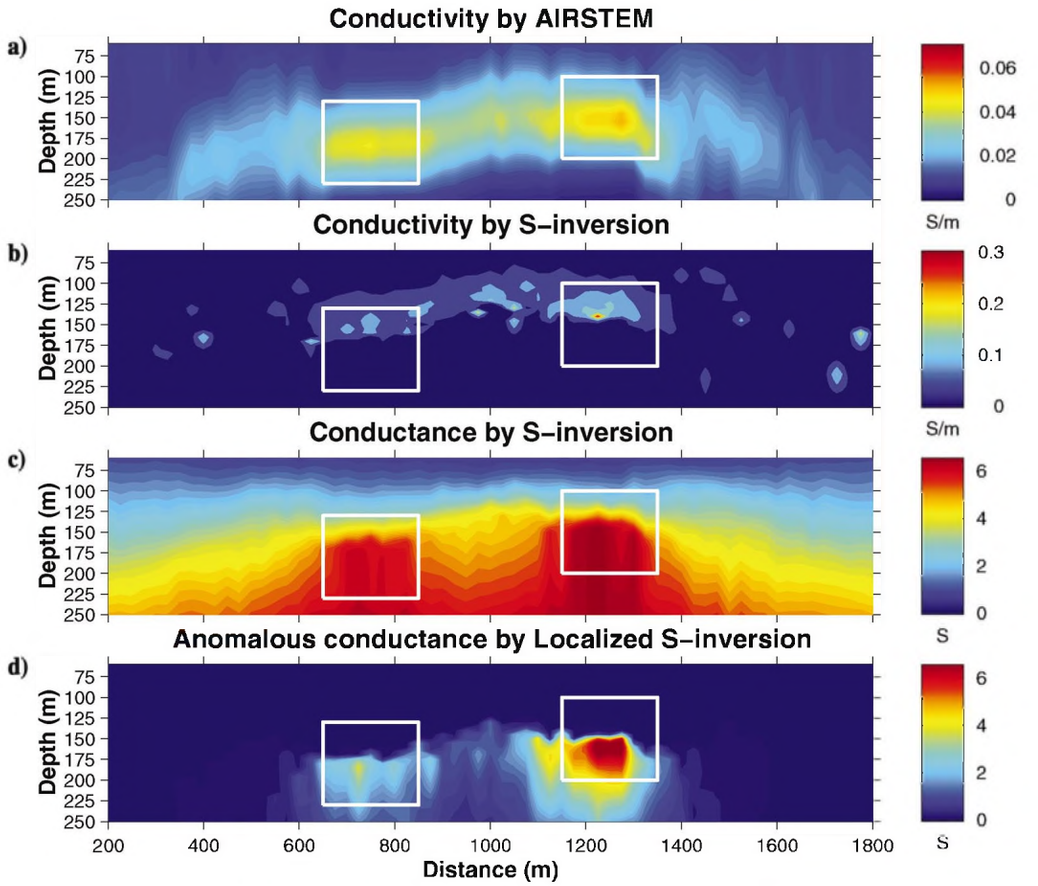

FIG. 10. Results of 1-D inversion, S-inversion, and localized S-inversion for model 2. (a) Result of the conventional smooth 1-D inversion by Airstem code. (b) Conductance cross-section by S-inversion. (c) Conductivity cross-section by S-inversion. (d) Anomalous conductance cross-section by localized S-inversion.

This mineralization zone is highly conductive; however, the presence of the conductive cover makes it difficult to locate by airborne EM observations.

The data set consists of one profile of airborne $dB_z(t)/dt$ field measured in 127 points with an interval of approximately 15 m. The length of the profile is about 2 km. There are 20 time channels, with 16 of them in the off-time interval. Figure 11 shows the profiles of the observed data, $dB_z(t)/dt$, for the different time channels.

The signal waveform in the transmitter $w(t)$ was provided with the data. According to formula (22), we used the convolution between the theoretical predicted data and the function $w(t)$ to account for the transmitter waveform in the inversion calculation. We used data only from the off-time channels.

Figure 12 presents the results of the inversion of the Bull Creek prospect airborne data. The flight elevation is shown by the blue dashed line in all four panels. Figure 12a presents the results of the conventional smooth 1-D inversion. We can clearly see a good conductor in this profile which corresponds to the known mineralization zone. Figure 12b shows a cross-section of the total conductance obtained by the original *S*-inversion. Figure 12c represents a conductivity cross-section obtained by the original *S*-inversion. We can see some conductive structures in the middle part of the profile in this image, but they are not clearly resolved. The result of the localized *S*-inversion (Figure 12d) produces a clearer image of the conductive targets in the anomalous conductance cross-section. We can distinguish a conductive zone in the middle part of the profile, which is associated with the known mineralization zone. Note that the image of the conductive zone presented in the bottom panel has much smaller horizontal extent than the corresponding image in the cross-section, obtained by 1-D inversion (top panel). This result corresponds well to the known geological characteristic of the mineralization zone (Hart and Lane, 2001). In particular, we show by the pink line the position of the borehole, which intersected a mineralization zone of valuable magnetite–pyrrhotite–pyrite content.

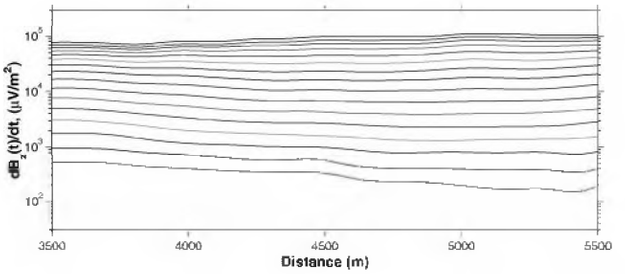

FIG. 11. The profiles of the airborne data $dB_z(t)/dt$ for different time channels collected at the Bull Creek prospect. Sixteen off-time channels are shown.

DISCUSSION AND CONCLUSION

We have developed the basic principles and theory of the localized *S*-inversion method. The method is based on an approximation of the conductivity cross-section by means of a horizontal conductive thin sheet consisting of a homogeneous background part and an inclusion formed by a local conductive disk with excess conductance ΔS. The localized *S*-inversion determines the distribution of this excess conductance as a function of the depth and a horizontal coordinate. The new method accounts for the limited horizontal extent of the inhomogeneities, localizing the inversion. The numerical model and the case history for an airborne TDEM data set show that the method better resolves the local mining geoelectrical targets than traditional 1-D inversion or original *S*-inversion. At the same time, *S*-inversion serves as the required first step of the localized *S*-inversion.

Further development of the localized *S*-inversion will require solving several problems. First, it is important to present the results of the localized *S*-inversion in the form of conductivity cross-sections, similar to 1-D or original *S*-inversion. Unfortunately, it is difficult to solve this problem by simply differentiating the conductance versus depth curves, as we could see with the examples presented in this paper. Second, the accuracy of the localized *S*-inversion can be improved by using a more accurate calculation of the conductive disk response than the Born approximation. Third, one can consider a more complicated model of the local conductive anomaly than a conductive disk model. All of these modifications could improve the practical efficiency of the localized *S*-inversion for interpreting TDEM data over 3-D inhomogeneous geoelectrical structures while preserving the basic simplicity of this method.

ACKNOWLEDGMENTS

We are thankful to BHP Research for funding this project and to BHP Minerals for providing the real TDEM data and granting permission to publish the results.

The authors also acknowledge the support of the University of Utah Consortium on Electromagnetic Modeling and Inversion (CEMI), which includes Advanced Power Technologies Inc., AGIP, Baker Atlas Logging Services, BHP Minerals, ExxonMobil Upstream Research Company, INCO Exploration, Japan National Oil Corporation, MINDECO, Naval Research Laboratory, Rio Tinto-Kennecott, 3JTech Corporation, and Zonge Engineering.

REFERENCES

Ellis, R. G., 1998a, Inversion of airborne electromagnetic data: Expl. Geophys., **29**, 121–127.

———1998b, Inversion of airborne electromagnetic data: 68th Ann. Internat. Mtg., Soc. Expl. Geophys., Expanded Abstracts, 2016–2019.

Habashy, T. M., Groom, R. W., and Spies, B. R., 1993, Beyond the Born and Rytov approximations: A nonlinear approach to electromagnetic scattering: J. Geophys. Res., **98**, No. B2, 1759–1775.

Hart, J., and Lane, R., 2001, Comparison of airborne and ground TEM systems for a conductor beneath conductive cover—An example from North-West Queensland, Australia: 15th Geophys. Conf. Austral. Soc. Expl. Geophys., Extended Abstracts.

Liu, G., and Asten, M., 1993, Conductance-depth imaging of airborne TEM data: Expl. Geophys., **24**, 655–662.

Nabighian, M. N., 1979, Quasi-static transient response of a conducting half-space—an approximate representation: Geophysics, **44**, 1700–1705.

Oristaglio, M. L., 1989, An inverse scattering formula that uses all the data: Inverse Prob., **5**, 1097–1105.

Sidorov, V. A., and Tikshaev, V. V., 1969, Electrical prospecting with transient field in near zone: Saratov University (in Russian).

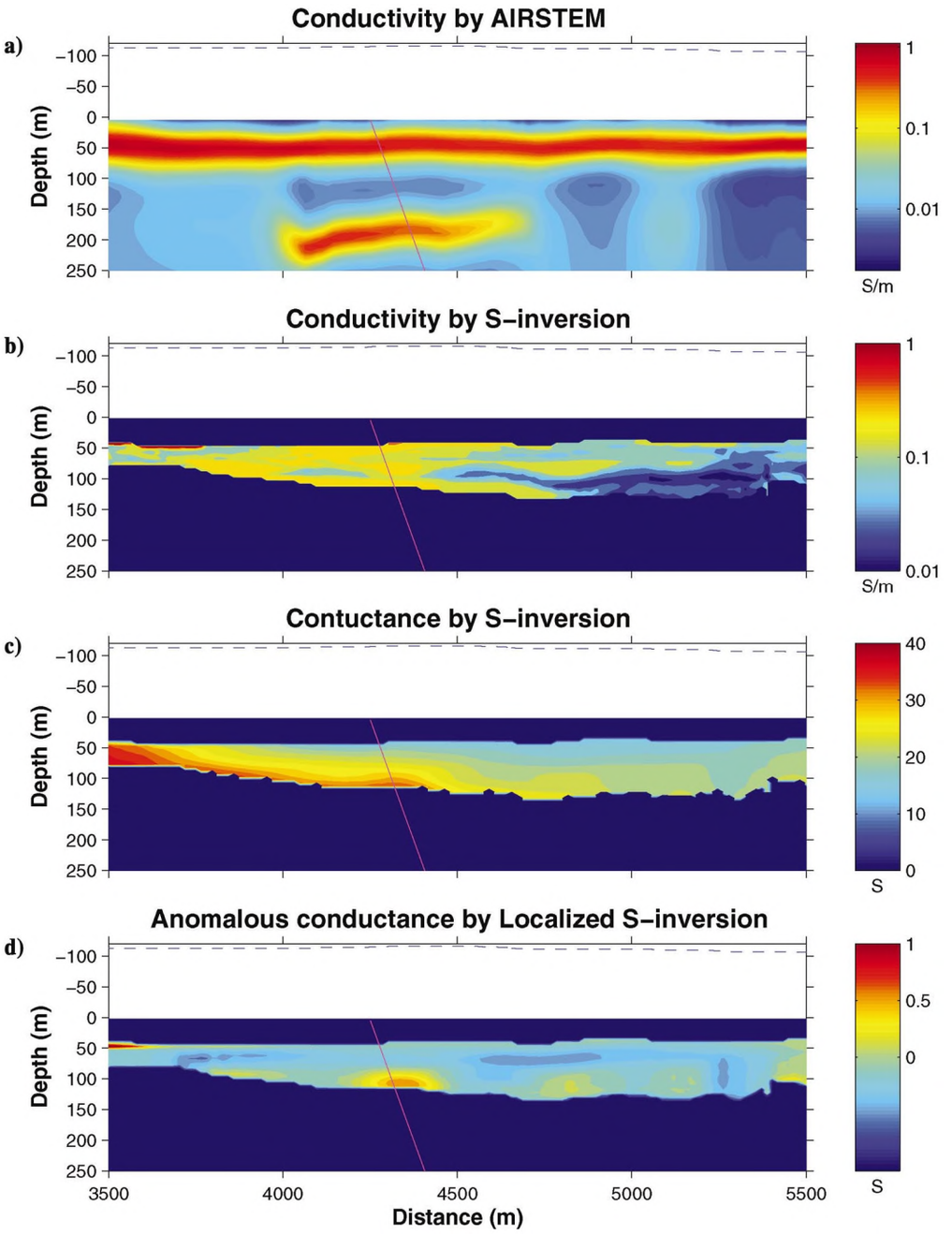

FIG. 12. Results of Bull Creek prospect airborne data inversion. (a) Result of the conventional smooth 1-D inversion by Airstem code. (b) Conductance cross-section by *S*-inversion. (c) Conductivity cross-section by *S*-inversion. (d) Anomalous conductance cross-section by localized *S*-inversion. The pink line shows the position of the borehole, which intersected a mineralization zone of valuable magnetite–pyrrhotite–pyrite content.

Tartaras, E., and Zhdanov, M. S., 1996, Fast *S*-inversion in the time domain: Method of interpretation using the thin sheet approach: 66th Ann. Internat. Mtg., Soc. Expl. Geophys., Expanded Abstracts, 1306–1309.

Tartaras, E., Zhdanov, M. S., Wada, K., Saito, A., and Hara, T., 2000, Fast imaging of TDEM data based on *S*-inversion: J. Appl. Geophys., **43**, No. 1, 15–32.

Xiong, Z., 1992, Electromagnetic modelling of three-dimensional structures by the method of system iterations using integral equations: Geophysics, **57**, 1556–1561.

Zhdanov, M. S., 1993, Tutorial: Regularization in inversion theory: Colorado School of Mines.

Zhdanov, M. S., and Keller, G. V., 1994, The geoelectrical methods in geophysical exploration: Elsevier Science Publ. Co., Inc.

APPENDIX

ELECTRIC FIELD OVER A THIN CONDUCTIVE SHEET

The components of an electric field at the surface of the conductive sheet ($z=0$), caused by a source excited with a Heaviside waveform, are

$$E_{x,y}(t)|_{z=0} = \frac{1}{2\pi}\int_{-\infty}^{\infty}\frac{1}{4\pi^2} \times \iint_{-\infty}^{\infty} e_{x,y}|_{z=0}\, e^{-i(k_x x+k_y y)}\, dk_x\, dk_y \times \left\{\pi\delta(\omega)-\frac{1}{i\omega}\right\} e^{-i\omega t}\, d\omega, \tag{A-1}$$

where $e_x|_{z=0}$ and $e_y|_{z=0}$ are the spatial spectra of the horizontal components of the electric field from the dipole source driven at a single harmonic frequency on the surface of the sheet ($z=0$). They can be found from the following expressions (Zhdanov and Keller, 1994):

$$e_x|_{z=0} = ik_x\psi, \tag{A-2}$$

$$e_y|_{z=0} = -ik_y\psi, \tag{A-3}$$

where

$$\psi = \psi(k_x, k_y, \omega) = M\frac{-i\omega\mu_0 e^{-n_0 d}}{2n_0 - i\omega\mu_0 S_b} \tag{A-4}$$

and where $n_0 = \sqrt{k_x^2 + k_y^2}$ and d is an elevation of the source above the thin sheet.

Therefore we can write

$$E_x(x,y,t) = -\frac{\partial}{\partial y}\Psi(x,y,t),\ E_y(x,y,t) = \frac{\partial}{\partial x}\Psi(x,y,t), \tag{A-5}$$

where

$$\Psi(x,y,t) = \frac{M}{8\pi^3}\int_{-\infty}^{\infty}\iint_{-\infty}^{\infty}\frac{\mu_0 e^{-n_0 d}}{2n_0 - i\omega\mu_0 S_b} \times e^{-i(k_x x+k_y y)}\, dk_x\, dk_y\, e^{-i\omega t}\, d\omega.$$

Interchanging the order of integration by spatial and time frequencies, we can write

$$\Psi(x,y,t) = \frac{M}{4\pi^2}\iint_{-\infty}^{\infty} A(t,n_0) e^{-i(k_x x+k_y y)}\, dk_x\, dk_y, \tag{A-6}$$

where $A(t, n_0)$ can be calculated using the residue theorem (Zhdanov and Keller, 1994, p. 381):

$$A(t,n_0) = \frac{\mu_0 e^{-n_0 d}}{2\pi}\int_{-\infty}^{\infty}\frac{e^{-i\omega t}}{2n_0 - i\omega\mu_0 S_b}\, d\omega = \frac{1}{S_b}\, e^{-2n_0\left(\frac{d}{2}+\frac{t}{\mu_0 S_b}\right)}. \tag{A-7}$$

Substituting equation (A-7) back into equation (A-6) and using the tabulated integral

$$\frac{1}{2\pi}\iint_{-\infty}^{\infty}\frac{1}{n_0}\, e^{-n_0|z|} e^{-i(k_x x+k_y y)}\, dk_x\, dk_y = \frac{1}{\sqrt{x^2+y^2+z^2}},$$

we obtain

$$\Psi(x,y,t) = -\frac{M}{4\pi^2 S_b}\frac{\mu_0 S_b}{2}\frac{\partial}{\partial t}\iint_{-\infty}^{\infty}\frac{e^{-2n_0\left(\frac{d}{2}+\frac{t}{\mu_0 S_b}\right)}}{n_0} \times e^{-i(k_x x+k_y y)}\, dk_x\, dk_y = -\frac{M\mu_0}{8\pi^2} \times \frac{\partial}{\partial t}\left[\frac{2\pi}{\sqrt{x^2+y^2+\left(d+\frac{2t}{\mu_0 S_b}\right)^2}}\right]. \tag{A-8}$$

After calculating the time derivative we can write

$$\Psi(x,y,t) = \frac{M}{2\pi S_b} d_\tau \left(x^2+y^2+d_\tau^2\right)^{-3/2}, \tag{A-9}$$

where the time-domain elevation d_τ is

$$d_\tau = d + \frac{2t}{\mu_0 S_b}. \tag{A-10}$$

Now we finally determine the electric-field components by substituting equation (A-9) into equation (A-5):

$$E_x(x,y,t) = -\frac{\partial}{\partial y}\Psi(x,y,t) = \frac{3M}{2\pi S_b} d_\tau \left(x^2+y^2+d_\tau^2\right)^{-5/2} y, \tag{A-11}$$

$$E_y(x,y,t) = \frac{\partial}{\partial x}\Psi(x,y,t) = -\frac{3M}{2\pi S_b} d_\tau \left(x^2+y^2+d_\tau^2\right)^{-5/2} x.$$